Strain, torsion and refractive index sensors based on helical long period fibre grating inscribed in small-core fibre for structural condition monitoring

Journal:	*Advances in Structural Engineering*
Manuscript ID	ASE-20-0572
Manuscript Type:	FRP-SSC – Special Issue
Date Submitted by the Author:	02-Aug-2020
Complete List of Authors:	Fu, Cailing; The Hong Kong Polytechnic University, Department of Civil and Environmental Engineering, Ni, YQ; The Hong Kong Polytechnic University, Department of Civil and Environmental Engineering Sun, Tong ; City University of London, Department of Electrical and Electronics Engineering Wang, Yiping; Shenzhen University DING, Siqi; The Hong Kong Polytechnic University, Department of Civil and Environmental Engineering vidakovic, miodrag; City University of London
Keywords:	Fibre optics components., Sensors, Hydrogen-oxygen technique, Structural health monitoring, Helical long period fibre gratings
Abstract:	This study is intended to develop long period fibre grating sensors for potential applications in environmental and durability monitoring of coastal structures. High-quality helical long period fibre gratings (HLPFGs) are inscribed in different types of small-core single mode fibres (SMFs) by use of hydrogen-oxygen flame heating technique. A detailed investigation of the effect of core diameter on their transmission spectrum and optimum length of the HLPFG has been pursued. A longer length is required to achieve the same coupling attenuation in a smaller-core SMF than that of a larger-core fibre. The strain, torsion and refractive index (RI) properties of the HLPFG is investigated experimentally to develop a high-sensitivity sensor. The experimental results show that the strain sensitivity could be enhanced by means of employing a larger-core diameter SMF. Moreover, the HLFPGs are also sensitive to the torsion and external RI. Hence, such HLFPGs have great potential for sensing applications.

Strain, torsion and refractive index sensors based on helical long period fibre grating inscribed in small-core fibre for structural condition monitoring

Cailing Fu [1, 2], Yi-Qing Ni [1, *], Tong Sun [3], Yiping Wang [2], Siqi Ding [1], Vidakovic Miodrag [3]

[1]Department of Civil and Environmental Engineering, The Hong Kong Polytechnic University, Hung Hom, Kowloon, Hong Kong, China.

[2]Guangdong and Hong Kong Joint Research Center for Optical Fibre Sensors, College of Physics and Optoelectronic Engineering, Shenzhen University, Shenzhen 518060, China.

[3]Department of Electrical and Electronics Engineering, City, University of London, London EC1V 0HB, England.

[*]Corresponding author: ceyqni@polyu.edu.hk

Abstract

This study is intended to develop long period fibre grating sensors for potential applications in environmental and durability monitoring of coastal structures. High-quality helical long period fibre gratings (HLPFGs) are inscribed in different types of small-core single mode fibres (SMFs) by use of hydrogen-oxygen flame heating technique. A detailed investigation of the effect of core diameter on their transmission spectrum and optimum length of the HLPFG has been pursued. A longer length is required to achieve the same coupling attenuation in a smaller-core SMF than that of a larger-core fibre. The strain, torsion and refractive index (RI) properties of the HLPFG is investigated experimentally to develop a high-sensitivity sensor. The experimental results show that the strain sensitivity could be enhanced by means of employing a larger-core diameter SMF. Moreover, the HLFPGs are also sensitive to the torsion and external RI. Hence, such HLFPGs have great potential for sensing applications.

Key words: Fibre optics components, sensors, helical long period fibre gratings, structural health monitoring, hydrogen-oxygen technique.

Introduction

Optical fibre sensor based on conventional fibre Bragg grating and long period fibre grating has been used to monitor various parameters such as temperature (Pei et al., 2016), strain (Lau et al., 2001), moisture (Sun et al., 2012), and pH (Ni et al., 2019, Nguyen et al., 2014) for health monitoring of civil engineering structures. However, the sensors based on helical long period fibre grating (HLFPG) have not been reported yet. The HLFPG with periodic screw-type refractive index (RI) modulation along the fibre axis has attracted great attention in various fields, such as orbital angular momentum (OAM) mode generator (Xi et al., 2014, Fu et al., 2018a), all-fibre circular polarization filter (Zhu et al., 2018), band-rejection filter (Inoue et al., 2016, Shin et al., 2007), torsion (Zhang et al., 2016, Xi et al., 2013) or RI sensors (Wang and Li, 2016, Ren et al., 2016) due to its unique properties. To date, various inscription methods, such as those using fibre drawing tower (Wong et al., 2012), electric arc discharge (Li et al., 2018a, Sun et al., 2017), CO_2 laser irradiation (Oh et al., 2004), and hydrogen-oxygen flame heating (Fu et al., 2018b, Li et al., 2018b), have been proposed and demonstrated to inscribe HLPFGs in different types of fibres, such as single mode fibre (SMF) (Fu et al., 2018b), few-mode fibre (FMF) (Zhao et al., 2019, Zhang et al., 2019), multi-core fibre (Shen et al., 2017), polarization-maintaining fibre (Jiang et al., 2019), photonic crystal fibre (PCF) (Fu et al., 2018a, Xi et al., 2014), and photonic band-gap fibre (Li et al., 2018a). Among these devices, the researchers focused on the characteristics of generating OAM mode based on these HLPFGs. For example, Xi et al. demonstrated the generation of the $OAM_{\pm1}$ modes based on a HLPFG in three-bladed Y-shaped core PCF (Xi et al., 2014). Recently, the authors also experimentally demonstrated an OAM_{+1} and $OAM_{\pm6}$ mode generators based on HLPFGs in SMF and PCF, respectively, by use of hydrogen-oxygen flame heating technique (Fu et al., 2018b, Fu et al., 2018a). Moreover, the sensing properties of the HLPFG in SMF with different cladding diameters by adjusting the relative velocity values of two translation stages were also demonstrated and compared (Li et al., 2018b, Zhao et al., 2020). However, the sensing responses to strain, torsion, RI and their dependence on the size of the core diameter have not been completely investigated yet.

In this work, the HLPFG samples are fabricated in SMF with different core diameters by use of the hydrogen-oxygen flame heating technique. The effect of the core diameter on transmission spectrum and the optimum length of the HLFPG were investigated experimentally. The strain, torsion, and external RI properties of $HLPFG_1$, $HLPFG_2$, and $HLPFG_3$ with a core diameter of 7.5, 4.2, and 3.6 μm, respectively, were investigated to develop a high-sensitivity sensor. Moreover, their sensing sensitivity dependence on the size of the core diameter was also discussed.

HLPFG Fabrication

As shown in Figure 1(a), a hydrogen-oxygen flame heating system, consisting of a fibre rotation motor, two translation stages, and a hydrogen-oxygen flame generator, was used to fabricate the HLPFGs. In the experiment, three types of SMFs with an original cladding diameter of 125 μm and core diameter of 9.0, 5.1, and 4.4 μm, respectively, were employed to inscribe HLPFGs. The detailed fabrication procedures to inscribe the HLPFG by use of hydrogen-oxygen technique are exactly the same as the ones that reported (Fu et al., 2018b). Note that in the experiment the velocity of two translation stages, i.e., V_1 and V_2, were set as 1.33 and 1.60 mm/s, then the helical pitch (Λ) could be calculated by the equation $\Lambda = 60V_2/\Omega$, where Ω is the rotational speed of the fibre rotation motor. Each end of the achieved HLPFGs was spliced with a SMF to measure the transmission spectrum by use of a broadband light source and an optical spectrum analyzer.

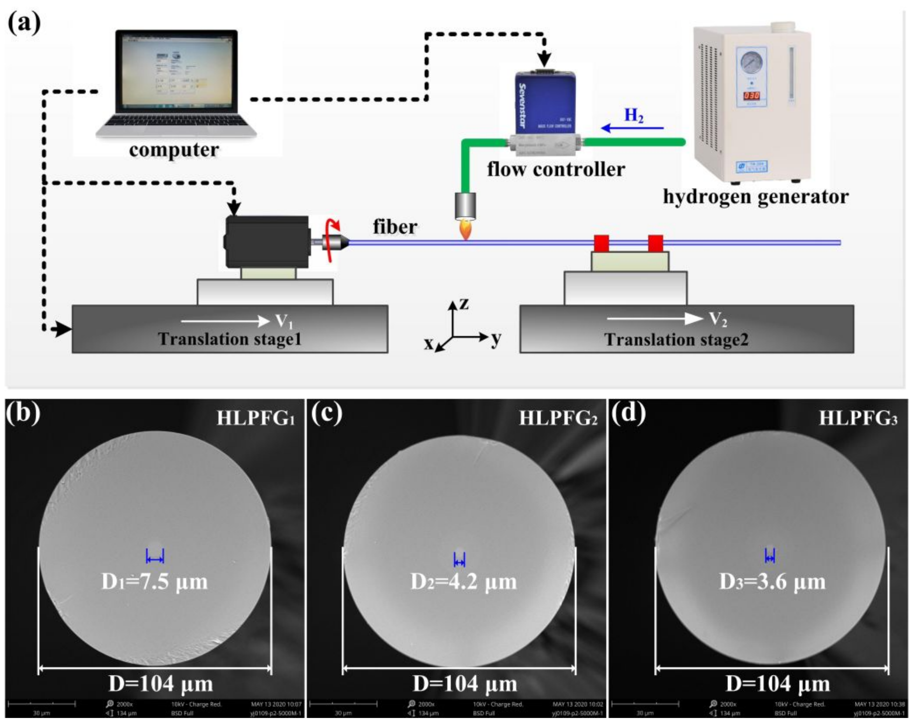

Figure 1. (a) Experimental setup for inscribing HLPFGs in SMF by use of hydrogen-oxygen flame heating technique; (b)-(d) Scanning electron micrographs of the cross section of achieved three HLPFGs, i.e., $HLPFG_1$, $HLPFG_2$, and $HLPFG_3$, with a reduced cladding diameter of 104 μm and core diameter of (b) D_1 = 7.5 μm, (c) D_2 = 4.2 μm, and (d) D_3 = 3.6 μm inscribed in SMFs with an original cladding diameter of 125 μm and core diameter of 9.0, 5.1, and 4.4 μm, respectively.

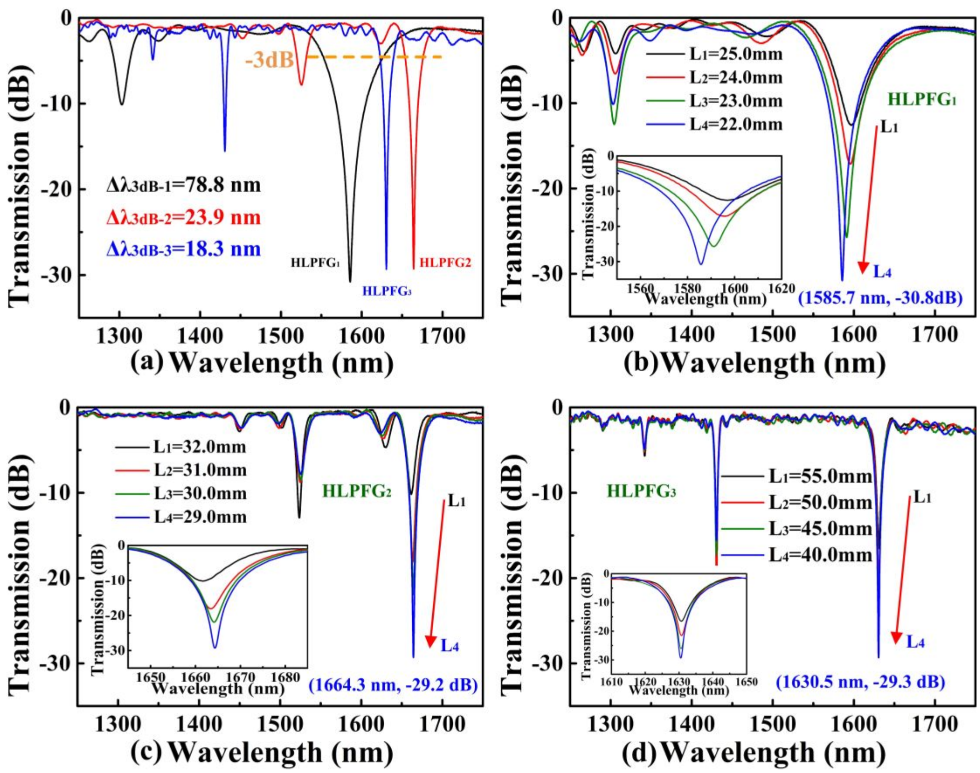

Figure 2. (a) Transmission spectra of three HLPFGs, i.e., $HLPFG_1$, $HLPFG_2$, and $HLPFG_3$, with the helical pitch of 518.9 μm inscribed in three types of SMFs; Transmission spectrum evolution of (b) $HLPFG_1$, (c) $HLPFG_2$, and (d) $HLPFG_3$ with a grating length decrease from L_1 to L_4. Inset illustrates the transmission spectrum evolution within a larger wavelength range.

To investigate the effect of the fibre core diameter on the transmission spectrum, three HLPFGs, i.e., $HLPFG_1$, $HLPFG_2$, and $HLPFG_3$, with the same helical pitch of 518.9 μm by applying a rotation speed of 185 rpm, were successfully inscribed in three types of SMFs with an original cladding diameter of 125 μm and core diameter of 9.0, 5.1, and 4.4 μm, respectively. Figure. 2(a) shows transmission spectra of three HLPFGs. As shown in Figures. 2(b), 2(c) and 2(d), the achieved $HLPFG_1$, $HLPFG_2$, and $HLPFG_3$ exhibited a reduced cladding diameter of 104 μm and core diameter of 7.5, 4.2, and 3.6 μm, respectively, which are attributed to the velocity difference between two translation stages, i.e., 1.60 and 1.33 mm/s. In addition, no physical deformation was observed on the surface of the achieved HLPFG, as previously reported (Fu et al., 2018b).

The transmission spectra of $HLPFG_1$ with a core diameter of 7.5 μm was illustrated in Figure. 2(a), while gradually decreasing its length from 25.0 to 22.0 mm with a step of 1 mm using a computer-controlled precision cleaving system. The resonant wavelength shifted toward a shorter wavelength, and the resonant dip of coupling attenuation increased gradually with the decrease of the HLPFG length. It is well known that the HLPFG has an optimum length, corresponding to the maximum coupling attenuation at the resonant wavelength (Fu et al., 2018a). As shown in Figure. 2(b), the optimum length of the $HLPFG_1$ was 22.0 mm, where the coupling attenuation was -30.8 dB at the resonant wavelength of 1585.7 nm. Compared with the $HLPFG_1$, the $HLPFG_2$ with a core diameter of 4.2 μm exhibited a longer optimum length of 29.0 mm when the resonant wavelength and coupling attenuation are 1664.3 nm and -29.2 dB, respectively, as illustrated in Figure. 2(c). The resonant wavelength of $HLPFG_2$ shifted toward a longer wavelength with the decrease of the length, which is opposite to that of $HLPFG_1$. Compared with $HLPFG_1$ and $HLPFG_2$, the optimum length of the $HLPFG_3$ with a core diameter of 3.6 μm was increased to 40 mm, but the resonant wavelength was remained at 1630.5 nm. Thus, the same fabrication parameters, i.e., the flow rate generated by the hydrogen generator and helical pitch, induced a stronger periodic RI modulation along the fibre axis in a larger-core fibre (7.5 μm) than that of smaller-core fibre (4.2, and 3.6 μm), indicating that the smaller core diameter of the HLPFG, the longer length to achieve the same coupling attenuation. In other words, a longer length is required to achieve the same coupling attenuation in a smaller-core SMF than that a larger-core fibre. Moreover, the 3dB-bandwidth of $HLPFG_1$ was 78.8 nm, as illustrated in Figure. 2(a), while that of

$HLPFG_2$ and $HLPFG_3$ was 23.9 and 18.3 nm, respectively. It is obvious that the 3dB-bandwidth could be narrowed by decreasing the core diameter of the fibre, which is in good agreement with previously reported results (Fu et al., 2015). Furthermore, an obvious interference could be observed on the transmission spectrum of $HLPFG_2$ and $HLPFG_3$ due to the mismatch of core diameter between the HLPFG sample and standard SMF, as illustrated in Figures. 2(c) and 2(d).

Strain response of the HLPFGs

Firstly, the strain responses of the achieved HLPFGs in SMF with different core diameters, i.e., $HLPFG_1$, $HLPFG_2$, and $HLPFG_3$, were measured to investigate the effect of core diameter on the strain response. In the experiment, one end of the HLPFG sample was fixed, another end was attached to a translation stage which was used to apply the strain along the fibre axis. When the HLPFG is stretched along the fibre axis, its helical pitch will be enlarged, resulting in the resonant wavelength shift. Therefore, the resonant wavelength of the $HLPFG_1$, $HLPFG_2$, and $HLPFG_3$ were measured while the strain was increased from 0 to 1800 με with a step of 100 με. As shown in Figures. 3(a), 3(b), and 3(c), the resonant wavelength of the $HLPFG_1$, $HLPFG_2$, and $HLPFG_3$ with different core diameters all shifted toward a shorter wavelength with the increase of the strain. As shown in Figures. 3(d), 3(e) and 3(f), the $HLPFG_1$, $HLPFG_2$, and $HLPFG_3$ exhibited a strain sensitivity of 1.35, 1.08, and 0.4 pm/με, respectively. Obviously, the strain sensitivity of the HLPFG with a larger core diameter, i.e., $HLPFG_1$, is two times higher than that of a smaller core diameter, i.e., $HLPFG_3$, indicating that the larger core diameter of the fibre, the higher the strain sensitivity. In other words, the strain sensitivity of the HLPFG is dependent on the size of the fibre core and could be enhanced by employing a larger-core diameter SMF.

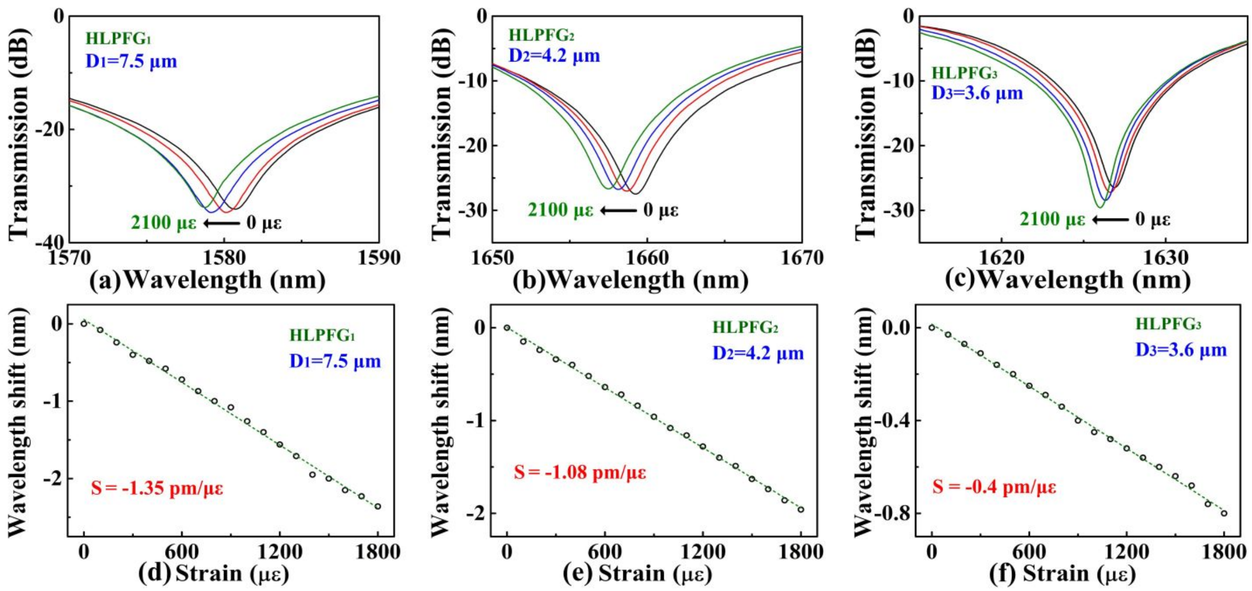

Figure 3. Transmission spectrum evolution of the (a) $HLPFG_1$, (b) $HLPFG_2$, and (c) $HLPFG_3$ sample with a core diameter of 7.5, 4.2, and 3.6 μm, respectively, while the strain increases from 0 to 1800 με; Measured resonant wavelength shift of the (d) $HLPFG_1$, (e) $HLPFG_2$, and (f) $HLPFG_3$ samples as a function of the strain.

Torsion response of the HLPFGs

To measure the mechanical torsion responses of the achieved HLPFGs in SMFs with different core diameter, two ends of the sample were fixed by a fibre rotator and fibre holder, where the distance between two fixed points, i.e., L, is 150 mm. During the measurement, the fibre rotator was clockwise or counter-clockwise rotated from 0^o to 300^o with a step of 30^o, i.e., the mechanical torsion rate of α_M varies from +0.035 to -0.035 rad/mm. Note that $\alpha_M > 0$ represented the clockwise torsion direction, while $\alpha_M < 0$ was the counter-clockwise torsion direction.

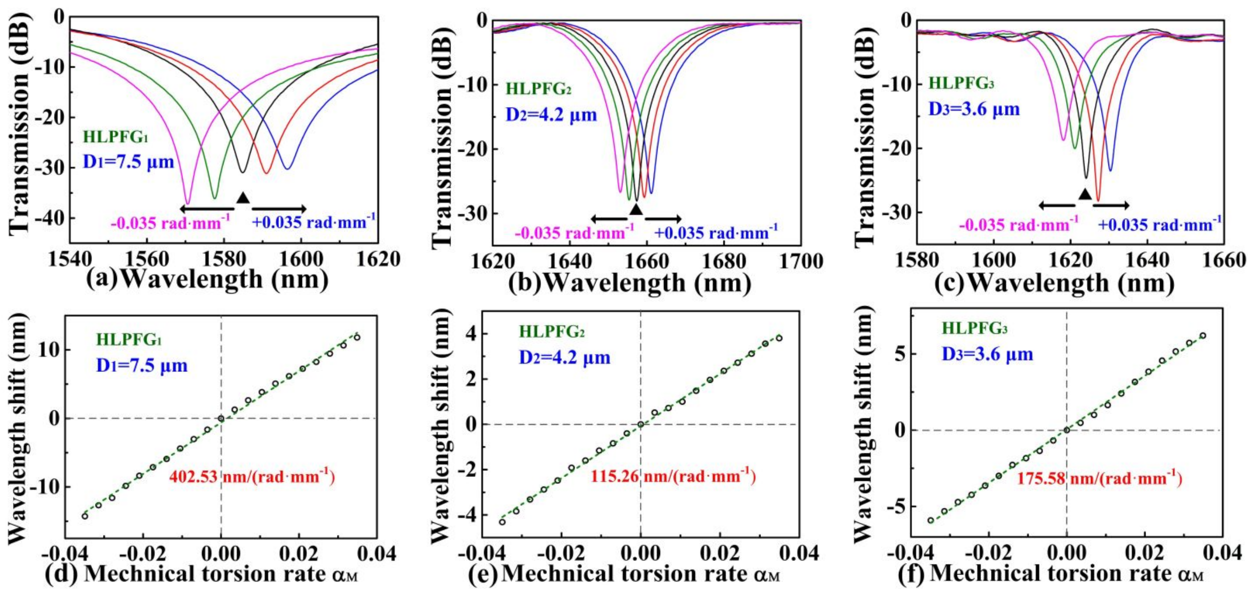

Figure 4. Transmission spectrum evolution of the (a) $HLPFG_1$, (b) $HLPFG_2$, and (c) $HLPFG_3$ sample with a core diameter of 7.5, 4.2, and 3.6 μm, respectively, while the mechanical torsion rate, α_M, changes from -0.035 to +0.035 rad/mm, and the original spectrum is shown in black; Measured resonant wavelength shift of the (d) $HLPFG_1$, (e) $HLPFG_2$, and (f) $HLPFG_3$ samples as a function of the mechanical torsion rate, α_M.

As shown in Figures. 4(a), 4(b), and 4(c), the resonant wavelength all exhibited a blue shift under the counter-clockwise mechanical torsion, while the opposite process occurred under the clockwise mechanical torsion. The original spectrum, i.e., $\alpha_M = 0$, was marked in black. And the total wavelength shift of $HLPFG_1$, $HLPFG_2$, and $HLPFG_3$ was 27.24, 8.12, and 12.12 nm, respectively. The measured resonant wavelength shift of the obtained HLPFGs, i.e., $HLPFG_1$, $HLPFG_2$, and $HLPFG_3$, as a function of the mechanical torsion rate was illustrated in Figures. 4(d), 4(e), and 4(f), showing a good linear relationship with a mechanical torsion sensitivity of 402.53, 115.26, and 175.58 nm/(rad·mm^{-1}), respectively. It is obvious that the mechanical torsion sensitivity of the $HLPFG_1$ with a larger core diameter of 7.5 μm is two times higher than that of the

$HLPFG_2$ with a smaller core diameter of 4.2 µm, instead of $HLPFG_3$ with a core diameter of 3.6 µm. In other words, the mechanical torsion sensitivity of the HLPFG is dependent on the size of the core diameter, but not linearly dependent. As previously reported, the direction of the mechanical torsion could be identified by observing the red or blue shift of the resonant wavelength, indicating that the obtained HLPFG could be used for structural health and condition monitoring.

Refractive index response of the HLPFGs

Finally, the external RI responses of the $HLPFG_1$, $HLPFG_2$, and $HLPFG_3$, were also investigated. The HLPFGs were measured at room temperature by immersing the samples into a series of RI liquids ranging from 1.30 to 1.43 with a step of 0.01 (Cargille Lab). Note that the tested HLPFG sample should be clearly cleaned by use of the alcohol to eliminate the residual liquids on the surface of fibre after each test. The transmission spectrum evolution of the $HLPFG_1$, $HLPFG_2$, and $HLPFG_3$ was illustrated in Figures. 5(a), 5(b) and 5(c), respectively, while the surrounding RI increasing from 1.30 to 1.43. As shown in Figures. 5(d), 5(e), and 5(f), the resonant wavelength of the $HLPFG_1$ shifted quickly toward a shorter wavelength with a total wavelength shift of 24.5 nm with the increase of the external RI. In contrast, the change of external RI resulted in approximately 9.6 and 19.9 nm resonant wavelength shift for $HLPFG_2$ and $HLPFG_3$, respectively. Therefore, the $HLPFG_1$ with a larger core diameter of 7.5 µm is the most sensitive, while the $HLPFG_2$ with a core diameter of 4.2 µm, rather than $HLPFG_3$ with the smallest core diameter, i.e., 3.6 µm, is the least.

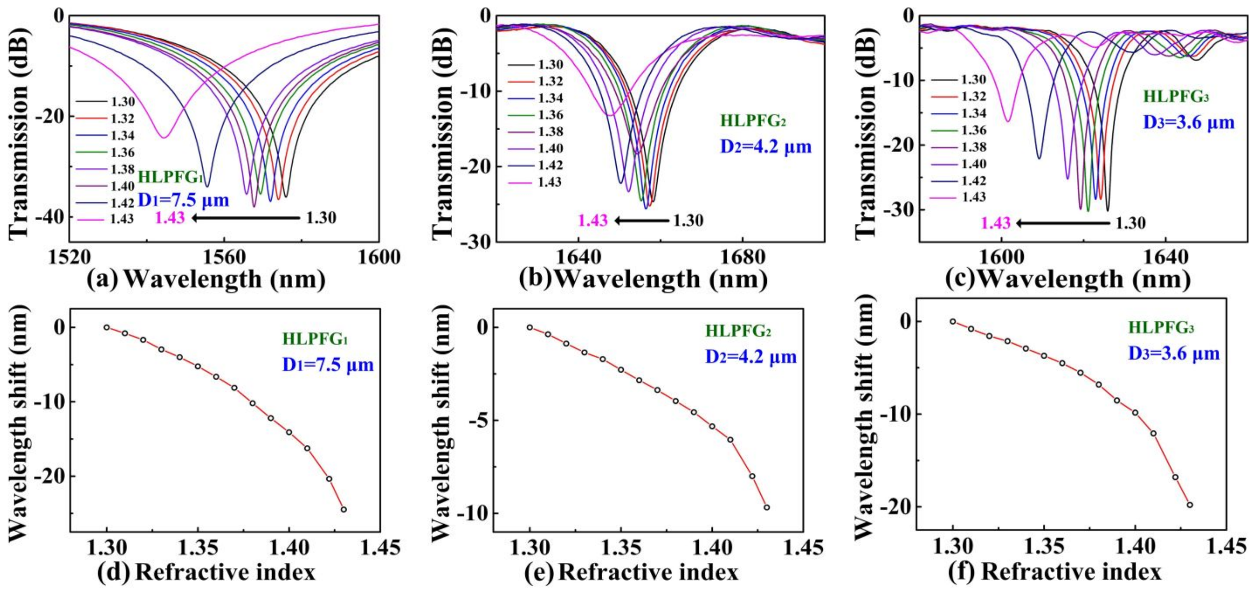

Figure 5. Transmission spectrum evolution of the (a) $HLPFG_1$, (b) $HLPFG_2$, and (c) $HLPFG_3$ sample with a core diameter of 7.5, 4.2, and 3.6 μm, respectively, while the external refractive changes from 1.30 to 1.43; Measured resonant wavelength shift of the (d) $HLPFG_1$, (e) $HLPFG_2$, and (f) $HLPFG_3$ samples as a function of the external RI.

Conclusions

The $HLPFG_1$, $HLPFG_2$, and $HLPFG_3$ samples with a core diameter of 7.5, 4.2, and 3.6 μm, respectively, are inscribed in three types of SMF with an original core diameter of 9.0, 5.1, and 4.4 μm, respectively, by use of the hydrogen-oxygen flame heating technique. The optimum length of the HLFPG is dependent on the core diameter, i.e., the smaller core diameter of the HLPFG, the longer length required to achieve the same coupling attenuation. The strain, mechanical torsion, and external RI properties of the obtained $HLFPG_1$, $HLPFG_2$, and $HLPFG_3$ were investigated. The experimental results show that the strain sensitivity, i.e., 1.35 pm/με, of $HLFPG_1$ is two times higher than that, i.e., 0.4 pm/με, of $HLPFG_3$. In contrast, the mechanical torsion of the $HLFPG_1$ is the most sensitive, i.e., 402.53, while the $HLFPG_3$ is the least 115.26, rather than the $HLPFG_2$, i.e., 175.58 nm/(rad·mm^{-1}). This experimental result also applied to the external RI sensing. The proposed HLFPGs could have great potential as optical sensors for a range of industrial applications including monitoring conditions inside seawater sea-sand concrete and fibre-reinforced polymer composites to enhance their integrity and sustainability.

Declaration of Conflicting Interests

The author(s) declared no potential conflicts of interest with respect to the research, authorship, and/or publication of this article.

Funding

The work described in this paper was supported by a grant (TRS) from the Research Grants Council of the Hong Kong Special Administrative Region, China (Project No. T22/502/18), a grant from the National Science Foundation of China (61905155), and a grant from The Hong Kong Polytechnic University (Project No. 1-BBAG). The authors would also like to appreciate the funding support by the Innovation and Technology Commission of the Hong Kong SAR Government (Project No. K-BBY1).

References

Fu CL, Liu S, Bai ZY, et al. (2018a). Orbital angular momentum mode converter based on helical long period Fibre grating inscribed by hydrogen-oxygen flame. *Journal of Lightwave Technology* 9(36): 1683-1688.

Fu CL, Liu S, Wang Y, et al. (2018b). High-order orbital angular momentum mode generator based on twisted photonic crystal fibre. *Optics Letters* 8(43): 1786-1789.

Fu CL, Zhong XY, Liao CR, et al. (2015). Thin-core-fiber-based long-period fiber grating for high-sensitivity refractive index measurement. *IEEE Photonics Journal* 6(7): 1-8.

Inoue G, Wang P,Li H (2016). Flat-top band-rejection filter based on two successively-cascaded helical fibre gratings. *Optics Express* 24(5): 5442-5447.

Jiang C, Liu YQ, Zhao YH, et al. (2019). Helical long-period gratings inscribed in polarization-maintaining fibers by CO_2 Laser. *Journal of Lightwave Technology* 37(3): 889-896.

Lau KT, Yuan LB, Zhou LM, et al. (2001). Strain monitoring in FRP laminates and concrete beams using FBG sensors. *Composite Structures* 51(1): 9-20.

Li J, Fan PC, Sun LP, et al. (2018a). Few-period helically twisted all-solid photonic bandgap fibres. *Optics Letters* 43(4): 655-658.

Li ZL, Liu S, Bai ZY, et al. (2018b). Residual-stress-induced helical long period fibre gratings for sensing applications. *Optics Express* 26(18): 24113-24122.

Nguyen TH, Venugopala T, Chen S, et al. (2014). Fluorescence based fibre optic pH sensor for the pH 10-13 range suitable for corrosion monitoring in concrete structures. *Sensors and Actuators B-Chemical* 191: 498-507.

Ni YQ, Ding SQ, Han BG, et al. (2019). Layer-by-layer assembly of polyelectrolytes-wrapped multi-walled carbon nanotubes on long period fibre grating sensors. *Sensors and Actuators B-Chemical* 301: 127120.

Oh ST, Lee KR, Paek UC, et al. (2004). Fabrication of helical long-period fibre gratings by use of a CO_2 laser. *Optics Letters* 29(13): 1464-1466.

Pei HF, Li ZJ,Li Y (2016). Early-age shrinkage and temperature optimization for cement paste by using PCM and MgO based on FBG sensing technique. *Construction and Building Materials* 117: 58-62.

Ren KL, Ren LY, Liang J, et al. (2016). Online fabrication scheme of helical long-period fibre grating for liquid-level sensing. *Applied Optics* 55(34): 9675-9679.

Shen X, Hu XW, Yang LY, et al. (2017). Helical long-period grating manufactured with a CO_2 laser on multicore fibre. *Optics Express* 25(9): 10405-10412.

Shin W, Yu BA, Noh YC, et al. (2007). Bandwidth-tunable band-rejection filter based on helicoidal fibre grating pair of opposite helicities. *Optics Letters* 32(10): 1214-1216.

Sun B, Wei W, Liao CR, et al. (2017). Automatic arc discharge-induced helical long period fiber gratings and its sensing applications. *IEEE Photonics Technology Letters* 29(11): 873-876.

Sun T, Grattan KTV, Srinivasan S, et al. (2012). Building stone condition monitoring using specially designed compensated optical fibre humidity sensors. *IEEE Sensors Journal* 12(5): 1011-1017.

Wang P and Li HP (2016). Helical long-period grating formed in a thinned fibre and its application to a refractometric sensor. *Applied Optics* 55(6): 1430-1434.

Wong GKL, Kang MS, Lee HW, et al. (2012). Excitation of orbital angular momentum resonances in helically twisted photonic crystal fiber. *Science* 337(6093): 446-449.

Xi XM, Wong GKL, Frosz MH, et al. (2014). Orbital-angular-momentum-preserving helical Bloch modes in twisted photonic crystal fibre. *Optica* 1(3): 165-169.

Xi X, Wong GKL, Weiss T, et al. (2013). Measuring mechanical strain and twist using helical photonic crystal fibre. *Optics Letters* 38(24): 5401-5404.

Zhang L, Liu YQ, Zhao YH, et al. (2016). High sensitivity twist sensor based on helical long-period grating written in two-Mode fiber. *IEEEPhotonics Technology Letters* 28(15): 1629-1632.

Zhang Y, Bai ZY, Fu CL, et al. (2019). Polarization-independent orbital angular momentum generator based on a chiral fibre grating. *Optics Letters* 44(1): 61-64.

Zhao H, Wang P, Yamakawa T, et al. (2019). All-fibre second-order orbital angular momentum generator based on a single-helix helical fibre grating. *Optics Letters* 44(21): 5370-5373.

Zhao YY, Liu S, Luo JX, et al. (2020). Torsion, refractive index, and temperature sensors based on an improved helical long period fiber grating. *Journal of Lightwave Technology* 38(8): 2504-2510.

Zhu CL, Yamakawa T, Zhao H, et al. (2018). All-fibre circular polarization filter realized by using helical long-period fiber gratings. *IEEE Photonics Technology Letters* 30(22): 1905-1908.